The following publication A. Stepanov, H. Saad, U. Karaagac and J. Mahseredjian, "Spurious Power Losses in Modular Multilevel Converter Arm Equivalent Model," in IEEE Transactions on Power Delivery, vol. 35, no. 1, pp. 205-213, Feb. 2020 is available at https://dx.doi.org/10.1109/TPWRD.2019.2911052.

Spurious Power Losses in Modular Multilevel Converter Arm Equivalent Model

Anton Stepanov, *Student Member, IEEE*, Hani Saad, *Member, IEEE*, Ulas Karaagac, *Member, IEEE*, Jean Mahseredjian, *Fellow, IEEE*

***Abstract*—This paper demonstrates the presence of spurious power losses or generation in the Arm Equivalent Model (AEM) of Modular Multilevel Converters. Such power losses can occur if model equations are not solved simultaneously with surrounding power circuit equations, which is the case when the AEM is implemented using control system blocks in an electromagnetic transient simulation software. Depending on operating conditions and simulation parameters, these additional losses can represent a significant part of the total converter station losses or even surpass them, thus making simulation results inaccurate.**

Analytical demonstration of the losses is presented, and several models that eliminate the losses are proposed. Based on simulation studies, only the variable resistance model and equivalent voltage source model can give accurate simulation results without significantly increasing simulation time and generating or consuming spurious power.

***Index Terms*—arm equivalent model, high-voltage direct current, losses, modeling, modular multilevel converter**

I. Introduction

The Modular Multilevel Converter (MMC) shown in Fig. 1 is a Voltage Source Converter (VSC) topology that has several advantages in comparison with conventional two- and three-level power electronic converters. Increasing the number of sub-modules (SMs) per arm helps to reduce or even eliminate filters, improve reliability and easily achieve scalability to higher voltages. In addition, MMCs have lower losses, switching frequency, transient peak voltages and switching voltages [1], [2]. During normal operation, the desired AC voltage waveform is constructed by inserting or bypassing the appropriate number of SMs [3].

Due to the increased structural complexity of this type of converter compared to the conventional VSCs, a larger set of models is applicable in electromagnetic transient (EMT) simulations, including detailed model (DM), detailed equivalent model (DEM), arm equivalent model (AEM) and average value model (AVM) [4]. The choice of the model depends on the given simulated phenomenon and is associated with a compromise between required accuracy and tolerable computational burden [5].

The models that include SM level details (DM and DEM) require relatively large simulation times when compared to the simplified counterparts due to increased complexity and smaller time-step usage (in the order of several μs or less) that is needed to achieve high accuracy [6]. The AEM represents all individual SMs as a single equivalent circuit (see Fig. 2), which makes this model advantageous for a large set of grid studies where the converter behavior on SM level is disregarded [7], [8]. Therefore, larger time-steps can be used (tens of μs) [6], [9].

The AEM can be implemented in different ways in an EMT-type software. The model equations can be incorporated into the main network equations (MNE), in which case the model equations can be solved simultaneously with the network. However, the main drawback is the inaccessibility of model equations to the user. Otherwise, the model equations can be implemented using control diagram blocks of the EMT software [10], [11]. In this case, the drawback is the one-time-step delay between the solution of control blocks and MNE in EMT-type software.

In this article it will be demonstrated that in the second approach (model in control blocks), additional spurious power losses can occur, that can affect the overall behavior of the circuit and make the simulation results less accurate. Similar phenomenon of additional losses has been reported in [12] for AVM but no detailed explanations have been provided. Therefore, analytical formulation of such losses for AEM is presented in this paper and solutions to remediate the problem are discussed. Proposed solutions are validated on a practical test case of an MMC-based HVDC transmission.

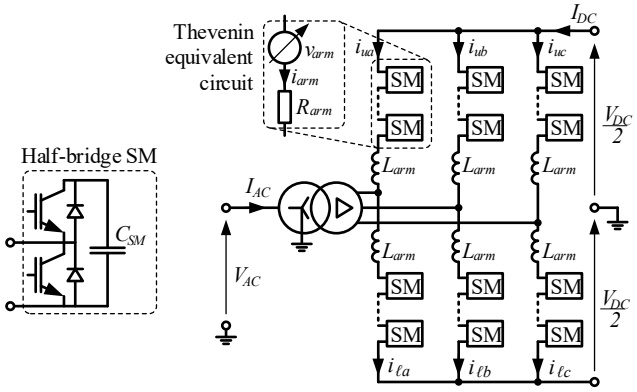

Fig. 1. Three-phase MMC topology with a coupling transformer.

A. Stepanov and J. Mahseredjian are with the Department of Electrical Engineering, Polytechnique Montréal, Montreal, QC H3T 1J4, Canada (email: anton.stepanov@polymtl.ca; jeanm@polymtl.ca).

H. Saad is with the Réseau de Transport d'Electricité, Paris 92932, France (e-mail: hani.saad@rte-france.com).

U. Karaagac is with the Department of Electrical Engineering, Hong Kong Polytechnic University, Hung Hom, Kowloon, Hong Kong (e-mail: ulas.karaagac@polyu.edu.hk).

This paper starts in section II with the presentation of main equations of the AEM. Section III demonstrates analytical derivation of spurious losses in steady-state. Solutions to eliminate spurious losses are proposed in section IV. The solutions are compared in steady-state and transient conditions using EMT simulations of 401-level MMC-HVDC system in section V.

II. Normal Operation of Arm Equivalent Model

Two operational modes are usually discussed when dealing with MMCs: normal operation and blocked mode. In this paper, normal operation is of primary interest, because power losses are important in steady-state operation [13].

To evaluate spurious power, let us consider an ideal AEM, i.e. lossless semiconductor devices (no switching or conducting losses). The basic equations of the model for a given arm during normal operation are as follows [4], [14]:

$$v_{arm}(t) = s(t)\, v_{Ctot}(t) \tag{1}$$

$$i_{Ctot}(t) = s(t)\, i_{arm}(t) \tag{2}$$

$$\frac{d}{dt} v_{Ctot}(t) = \frac{i_{Ctot}(t)}{C_{eq}} \tag{3}$$

$$C_{eq} = C_{SM} / N_{SM} \tag{4}$$

where s is the arm switching function, v_{arm} is the arm voltage, v_{Ctot} is the equivalent capacitor voltage, i_{arm} is the arm current, i_{Ctot} is the equivalent capacitor current, C_{eq} is the equivalent capacitor, C_{SM} is the SM capacitance and N_{SM} is the number of SMs per arm.

If equations (1)–(3) are solved simultaneously at each time-point, the solution is perfectly accurate, as demonstrated below. Instantaneous arm power on the power circuit side is given by:

$$P_{arm}(t) = i_{arm}(t)\, v_{arm}(t) \tag{5}$$

Instantaneous power on the equivalent capacitor side becomes:

$$P_{Ctot}(t) = i_{Ctot}(t)\, v_{Ctot}(t) \tag{6}$$

The powers in (5) and (6) must be equal, because there is no other element that can consume, produce or store energy (as semiconductor losses are not considered in this equation). Considering (2), (6) can be rewritten as

$$P_{Ctot}(t) = i_{arm}(t)\, s(t)\, v_{Ctot}(t) \tag{7}$$

When considering (1), (5), and (7) it is clear that $P_{arm}(t) = P_{Ctot}(t)$, so no spurious power losses occur irrespective of the waveforms of arm currents and voltages.

A. Classical AEM 1

Arm equations (1)–(3) can be implemented in an EMT-type simulation software in a form of a control circuit (Fig. 2). In this case, semiconductor conduction losses can be modeled with a constant resistance [4]:

$$R_{arm} = R_{ON}\, N_{SM} \tag{8}$$

where R_{ON} is the ON-state resistance of IGBT switches.

Instantaneous conduction losses are then expressed as

$$P_{COND}(t) = i_{arm}^2(t)\, R_{arm} \tag{9}$$

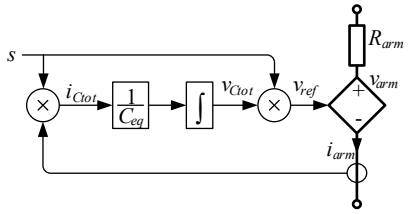

Fig. 2. Classical AEM 1 for normal operation mode.

B. Classical AEM 2

Another possible implementation of classical AEM from [4], [15] is shown in Fig. 3. Compared to the classical AEM 1, there is an additional time-step delay between i_{ref} and capacitor current i_{Ctot} introduced by the controlled current source. The capacitor is implemented as part of power circuit. Conduction losses (8) can also be included.

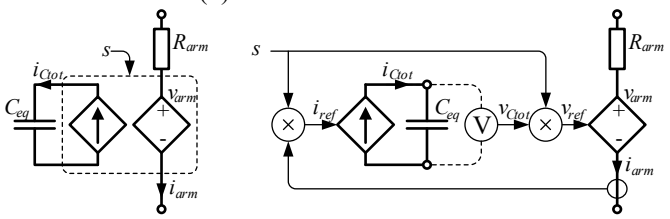

a) overview b) detailed diagram

Fig. 3. Classical AEM 2 (constant capacitor) for normal operation mode.

III. Spurious Losses of AEM in Steady-State

In EMT-type software codes it is usual to solve control system equations independently from MNE, which results in a one-time-step delay between the two solutions. As it will be demonstrated, this can result in spurious losses ΔP, which is defined as the difference between $P_{arm}(t)$ and $P_{Ctot}(t)$:

$$\Delta P(t) = P_{arm}(t) - P_{Ctot}(t) \tag{10}$$

A. Origin of Losses

1) Classical AEM 1

In EMT-type software implementation of classical AEM 1 shown in Fig. 2, there is a one-time-step (Δt) delay between v_{ref} (reference value from the control blocks), and v_{arm} (actual voltage):

$$v_{ref}(t) = v_{arm}(t + \Delta t) \tag{11}$$

Considering (11), (1) can be rewritten as

$$v_{arm}(t + \Delta t) = v_{ref}(t) = s(t)\, v_{Ctot}(t) \tag{12}$$

Considering (12), (7) is rewritten as

$$P_{Ctot\ AEM\,1}(t) = i_{arm}(t)\, v_{ref}(t) \tag{13}$$

Introducing (5), (11), and (13) into (10):

$$\Delta P_{AEM\,1}(t) = -i_{arm}(t)\left[v_{arm}(t + \Delta t) - v_{arm}(t)\right] \tag{14}$$

Clearly, as v_{arm} is not a constant value, the delay between controls blocks solution and MNE solution causes a difference between $P_{arm}(t)$ and $P_{Ctot}(t)$, which results in overall spurious power losses or generation (if negative value).

Assuming that simulation time-step is small, the arm voltage derivative at a time-point t can be approximated by the finite difference:

$$\frac{d}{dt}v_{arm}(t)\approx\frac{v_{arm}(t+\Delta t)-v_{arm}(t)}{\Delta t} \tag{15}$$

With (15), (14) is rewritten to simplify steady-state analysis:

$$\Delta P_{AEM\,1}(t)\approx-\Delta t\, i_{arm}(t)\frac{d}{dt}v_{arm}(t) \tag{16}$$

2) Classical AEM 2

Similarly, after algebraical manipulations, power at the capacitor side can be obtained for the classical AEM 2:

$$P_{Ctot\ AEM\,2}(t)=i_{arm}(t-\Delta t)\,v_{arm}(t+\Delta t)\frac{s(t-\Delta t)}{s(t)} \tag{17}$$

Spurious power losses for the classical AEM 2 can be derived from (17) as

$$\Delta P_{AEM\,2}(t)\approx\Delta t\, v_{arm}(t)\frac{d}{dt}i_{arm}(t) \tag{18}$$

For better precision, a supplementary term can be added:

$$\delta P_{AEM\,2}(t)\approx-\Delta t\, i_{arm}(t)\,v_{arm}(t)\frac{d}{dt}\frac{v_{Ctot}(t)}{V_{DC}} \tag{19}$$

The derivation of (17)–(19) is shown in the appendix.

B. Steady-State Spurious Losses

For high-power MMCs used in HVDC transmissions, it is typical to have high number of levels and double-fundamental frequency circulating current suppression control [16]. In this case, high-frequency components in arm voltages and currents can be neglected, as well as second-harmonic terms. Therefore, only DC and fundamental components will be considered in steady-state operation (in the following, indices 0, 1, and 2 represent the order of harmonic components):

$$i_{arm}(t)=I_0+I_1\cos(\omega t+\varphi_i) \tag{20}$$

$$v_{arm}(t)=V_0+V_1\cos(\omega t+\varphi_v) \tag{21}$$

where I_0, I_1, V_0, and V_1 are the amplitudes of the DC and the fundamental components of arm current and voltage respectively, φ_i and φ_v are the corresponding phase angles, and ω is the grid frequency in rad/s.

The values of spurious losses can be estimated using only (20) and (21). According to [17], derivative in (19) can be approximated:

$$\begin{aligned}\frac{d}{dt}v_{Ctot}(t)=&\frac{1}{C_{eq}}\left[\frac{I_1}{2}\cos(\omega t+\varphi_i)+\frac{I_0V_1}{V_{DC}}\cos(\omega t+\varphi_v)\right]\\&+\frac{1}{C_{eq}}\left[\frac{I_1V_1}{V_{DC}}\cos(2\omega t+\varphi_i+\varphi_v)\right]\end{aligned} \tag{22}$$

Considering (16)–(22), spurious losses for any given arm can be calculated as follows with classical AEMs:

$$\Delta P_{AEM\,1}(t)=\Delta t\left[I_0+I_1\cos(\omega t+\varphi_i)\right]\omega V_1\cos\left(\omega t+\varphi_v-\frac{\pi}{2}\right) \tag{23}$$

$$\Delta P_{AEM\,2}(t)\approx\Delta t\left[V_0+V_1\cos(\omega t+\varphi_v)\right]\omega I_1\cos\left(\omega t+\varphi_i+\frac{\pi}{2}\right) \tag{24}$$

The above equations can be separated into harmonic terms: DC components, fundamental components, and double-fundamental-frequency components. For classical AEM 1:

$$\Delta P_2^{AEM\,1}(t)=\Delta t\ \omega\frac{V_1I_1}{2}\cos\left(2\omega t+\varphi_v+\varphi_i-\frac{\pi}{2}\right) \tag{25}$$

$$\Delta P_1^{AEM\,1}(t)=\Delta t\ \omega V_1I_0\cos\left(\omega t+\varphi_v-\frac{\pi}{2}\right) \tag{26}$$

$$\Delta P_0^{AEM\,1}(t)=\Delta t\ \omega\frac{V_1I_1}{2}\cos\left(\varphi_v-\varphi_i-\frac{\pi}{2}\right) \tag{27}$$

$$\Delta P_{AEM\,1}(t)=\Delta P_2^{AEM\,1}(t)+\Delta P_1^{AEM\,1}(t)+\Delta P_0^{AEM\,1}(t) \tag{28}$$

For classical AEM 2:

$$\Delta P_2^{AEM\,2}(t)=\Delta t\ \omega\frac{V_1I_1}{2}\cos\left(2\omega t+\varphi_i+\varphi_v+\frac{\pi}{2}\right) \tag{29}$$

$$\Delta P_1^{AEM\,2}(t)=\Delta t\ \omega V_0I_1\cos\left(\omega t+\varphi_i+\frac{\pi}{2}\right) \tag{30}$$

$$\Delta P_{0\,part}^{AEM\,2}(t)=\Delta t\ \omega\frac{V_1I_1}{2}\cos\left(\varphi_v-\varphi_i-\frac{\pi}{2}\right) \tag{31}$$

$$\begin{aligned}\delta P_0^{AEM\,2}(t)=&-\frac{\Delta t}{C_{eq}}\left[\frac{V_0I_1^2}{4V_{DC}}+\frac{V_1^2I_0^2}{2V_{DC}^2}+\frac{V_1^2I_1^2}{8V_{DC}^2}\right]\\&-\frac{\Delta t}{C_{eq}}\left[\frac{V_1I_0I_1}{4V_{DC}}+\frac{V_0V_1I_0I_1}{2V_{DC}^2}\right]\cos(\varphi_v-\varphi_i)\end{aligned} \tag{32}$$

$$\Delta P_0^{AEM\,2}(t)=\Delta P_{0\,part}^{AEM\,2}(t)+\delta P_0^{AEM\,2}(t) \tag{33}$$

$$\Delta P_{AEM\,2}(t)=\Delta P_2^{AEM\,2}(t)+\Delta P_1^{AEM\,2}(t)+\Delta P_0^{AEM\,2}(t) \tag{34}$$

The oscillating terms (25), (26) or (29), (30) will not deteriorate steady-state power balance because all the extra-generated power during one half-cycle will be consumed during the other half-cycle. The constant term, however, will always be present and will affect the converter power balance.

1) Double-Fundamental-Frequency Spurious Losses

Under balanced conditions, double-fundamental-frequency components (25) (or (29) for classical AEM 2) in the lower arms sum up to zero due to the 120° phase shift in between them. The same can be said about upper arms, so these components have no effect outside of the MMC.

However, depending on control strategies during grid unbalance [16], fundamentals of current and voltage can differ among phases, so it is possible that double-fundamental-frequency spurious losses become visible outside the MMC.

2) Fundamental-Frequency Spurious Losses

In a given phase, the DC components of current and voltage in the upper and lower arm are identical, while the fundamental components have a 180° phase shift. Therefore, fundamental-frequency losses (26) (or (30)) in upper and lower arms cancel each other out in each phase, since they are in phase opposition. Unbalance between upper and lower arms in each phase is usually kept to a minimum even during grid unbalance, so there is no effect of these losses on the external behavior of the converter.

3) Constant Spurious Losses

The constant losses (27) (or (33)) are the source of power mismatch affecting the whole grid. Depending on the phases of the AC components of arm current and voltage, power generation can also occur. In balanced conditions, constant losses are the same for all six arms, so their effects sum up and can be observed outside of the MMC. During unbalance, the values can differ among arms.

IV. Elimination of Losses

Four types of solutions to remove the spurious losses are considered: time-step reduction, extrapolating voltage references (extrapolation AEMs), variable resistance AEM, and equivalent voltage source AEM.

A. Time-Step Reduction

According to (23) and (24), spurious power losses in classical AEMs are proportional to Δt. If it is supposed that having maximal spurious power losses below or equal to 10% of average conduction losses (9) (denoted as $P_{COND\,0}$) is satisfactory, the corresponding Δt can be found as:

$$\max\left|\Delta P_{AEM\,1}\right| \le 10\%\ P_{COND\,0} \tag{35}$$

$$\Delta t_{AEM\,1}\ \omega\, V_1\left[I_0 + I_1\right] \le 0.1\ R_{arm}\left[I_0^2 + I_1^2/2\right] \tag{36}$$

$$\Delta t_{AEM\,1} \le 0.1\frac{R_{arm}\left[I_0^2 + I_1^2/2\right]}{\omega\, V_1\left[I_0 + I_1\right]} \tag{37}$$

Similarly, the time-step for classical AEM 2 is:

$$\Delta t_{AEM\,2} \le 0.1\frac{R_{arm}\left[I_0^2 + I_1^2/2\right]}{\omega\, I_1\left[V_0 + V_1\right]} \tag{38}$$

With this criterion, for high-power HVDC transmissions where voltages can reach hundreds of kV and currents are in the order of kA, satisfactory reduction of losses can be achieved with time-steps not higher than 10 µs.

B. Extrapolation AEM 1

In steady-state and with relatively small simulation time-steps, arm voltage derivatives do not change significantly between adjacent time-points. This can justify a simple one-time-step extrapolation of the final voltage reference v_{ref}^{ext} supplied to the controlled voltage source:

$$v_{ref}^{ext}\left(t\right) = v_{ref}\left(t\right) + \Delta t\,\frac{d}{dt}v_{ref}\left(t\right) \tag{39}$$

$$v_{arm}\left(t\right) = v_{ref}^{ext}\left(t-\Delta t\right) \tag{40}$$

The reference voltage derivative in (39) can be represented in the vicinity of time-point *t* using Taylor series (O represents higher-order terms):

$$v_{ref}\left(t\right) = v_{ref}\left(t-\Delta t\right) + \Delta t\,\frac{d}{dt}v_{ref}\left(t-\Delta t\right) + O\left(\Delta t^2\right) \tag{41}$$

Finally, (14) is rewritten as follows:

$$\begin{aligned}\Delta P_{AEM\,1}\left(t\right) &= i_{arm}\left(t\right)\left[v_{ref}^{ext}\left(t-\Delta t\right) - v^{ref}\left(t\right)\right]\\ &= i_{arm}\left(t\right)O\left(\Delta t^2\right)\end{aligned} \tag{42}$$

In steady-state and with small time-steps, the second- and higher-order terms $O\left(\Delta t^2\right)$ are considerably smaller than the first-order derivative in (16), therefore $\Delta P_{AEM\,1}$ is significantly reduced. The derivative of the voltage reference in (39) can be approximated similarly to (15), so:

$$v_{ref}^{ext}\left(t\right) = 2v_{ref}\left(t\right) - v_{ref}\left(t-\Delta t\right) \tag{43}$$

The corresponding implementation is shown in Fig. 4.

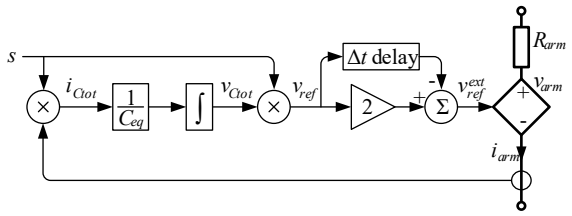

Fig. 4. Extrapolation AEM 1 diagram.

C. Extrapolation AEM 2

Based on the same assumptions, extrapolation can be applied to the classical AEM 2. In addition to (43), current source reference is defined as

$$i_{ref}^{ext}\left(t\right) = 2i_{ref}\left(t\right) - i_{ref}\left(t-\Delta t\right) \tag{44}$$

The corresponding implementation is shown in Fig. 5.

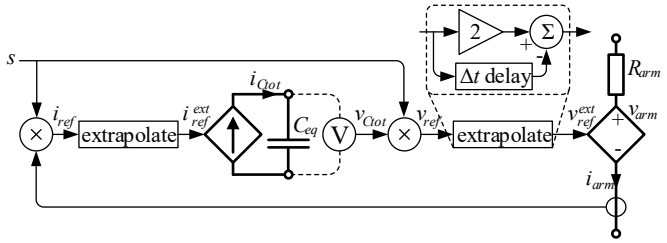

Fig. 5. Extrapolation AEM 2 diagram.

D. Variable Resistance AEM

Another solution is to include a current-dependent summand into the calculation of arm voltage. Discretization of (3) using trapezoidal integration yields

$$v_{Ctot}\left(t\right) = V_{hist\ Ctot}\left(t\right) + R_C\ i_{arm}\left(t\right)s\left(t\right) \tag{45}$$

with

$$V_{hist\ Ctot}\left(t\right) = v_{Ctot}\left(t-\Delta t\right) + R_C\ i_{arm}\left(t-\Delta t\right)s\left(t-\Delta t\right) \tag{46}$$

$$R_C = \frac{\Delta t}{2\,C_{eq}} \tag{47}$$

Multiplying both sides of (45) by $s(t)$ and considering (1):

$$v_{arm}\left(t\right) = R_C\ s^2\left(t\right)i_{arm}\left(t\right) + s\left(t\right)V_{hist\ Ctot}\left(t\right) \tag{48}$$

Since $V_{hist\ Ctot}\left(t\right)$ and $s\left(t\right)$ are known before the solution of MNE at the current time-point, implementation of (48) in the form of a Thevenin equivalent is straightforward:

$$V_{th}\left(t\right) = V_{hist\ Ctot}\left(t\right)s\left(t\right) \tag{49}$$

$$R_{th}\left(t\right) = R_C\ s^2\left(t\right) \tag{50}$$

In this case, arm equations (1)–(3) are all solved simultaneously due to the instantaneous contribution provided by the variable resistance, so no spurious power losses occur. Equations (45)–(50) can be implemented using standard

control diagram blocks, as shown in Fig. 6. However, this solution requires refactorization of MNE each time the value of R_{th} changes. It can be noted that $s(t)$ in (49) and (50) can be interpreted as a variable ideal transformer ratio.

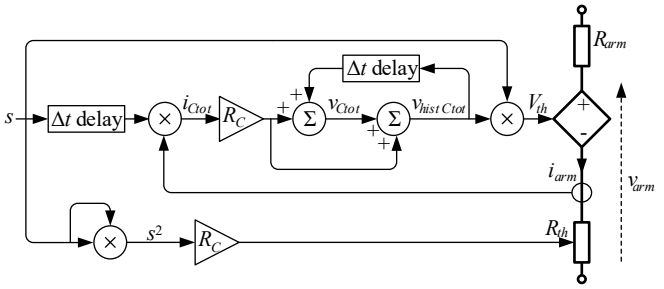

Fig. 6. Variable resistance AEM diagram.

E. Equivalent Voltage Source AEM

The solutions presented in previous sections IV.B and IV.D can be combined to overcome their inconveniences: instead of including a variable resistance to increase precision, its effect can be emulated by an equivalent voltage source $V_{R\,eq}$ so that there is no need to refactor the MNE each time the value of the switching function changes:

$$V_{R\,eq}(t) = R_{th}\, i_{arm}^{ext}(t) \tag{51}$$

where i_{arm}^{ext} is the extrapolated arm current.

This current can be obtained in a similar way to (44):

$$i_{arm}^{ext}(t) = 2i_{arm}(t) - i_{arm}(t-\Delta t) \tag{52}$$

The corresponding implementation is shown in Fig. 7.

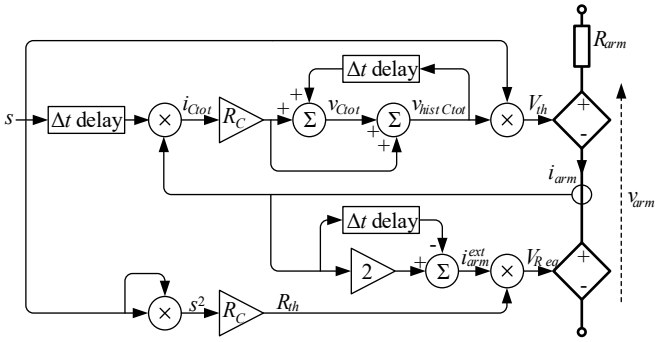

Fig. 7. Equivalent voltage source AEM diagram.

V. Simulation Results

A 401-level MMC-based HVDC link (Fig. 8) is used to validate the presented methods for eliminating spurious power losses. A standard cascade control system is used [5]. MMC1 controls active and reactive powers, MMC2 controls DC voltage and reactive power. System parameters are given in Table I. DC cable model details can be found in [4]. All simulations are performed in EMTP [18].

Total converter station losses with half-bridge MMCs amount to approximately 1% of its nominal power P_{nom} [19], whereas power losses in high power transformers can lie within 0.3%–0.5% range of its nominal power [20], the rest corresponds to the converter and auxiliary high voltage equipment losses [21]. The latter is relatively small (around 0.1% [21]) and is neglected in this study. So, the transformer losses are taken as 0.3% and the losses represented by arm resistances (8) are taken as 0.6% of P_{nom}.

The ON-state resistance R_{ON} of a single IGBT switch can be found from (53) at nominal power transfer. The obtained value is 2.304 mΩ, which is realistic for high power MMCs [21].

$$\frac{0.6}{100} P_{nom} = 6\, N_{SM}\, R_{ON} \left[I_0^{\,2} + \frac{I_1^{\,2}}{2} \right] \tag{53}$$

In the simulations, a 50 μs time-step is applied when AEMs are used. Having this relatively large time-step serves two purposes: to emphasize the problem and to demonstrate that even with a large Δt, accurate results can be obtained if loss-elimination methods are applied. The reference waveforms are obtained with the DEM using $\Delta t = 5\,\mu s$.

TABLE I
Simulation Parameters

Parameter	Nominal value	Symbol
Simulation time-step	50 μs	Δt
Grid frequency (both grids)	$2\pi \times 50$ rad/s	ω
Grid voltage (both grids)	400 kV	V_{AC}
Grid short-circuit level (both grids)	10 GVA	S_{SC}
DC voltage	640 kV	V_{DC}
Nominal MMC power (both stations)	1000 MW	P_{nom}
Number of SMs per arm (half-bridge)	400	N_{SM}
DC voltage reference	1 pu	
Reactive power reference (both stations)	0 pu	
ON-state resistance of IGBTs & diodes	2.304 mΩ	R_{ON}
Arm inductance	0.15 pu	L_{arm}
Transformer resistance	0.004 pu	
Transformer inductance	0.18 pu	
Capacitor energy	40 kJ/MVA	

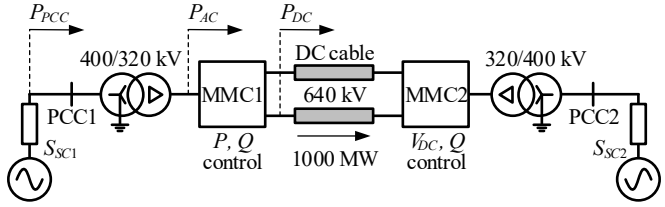

Fig. 8. Simulated point-to-point MMC-HVDC link.

A. Demonstration of Spurious Power Losses

To demonstrate the effects of spurious power losses, active powers at different points of the circuit are shown in Fig. 9 for the case of nominal power transfer using DEM and classical AEMs: at the point of coupling with the grid (P_{PCC}), at the AC terminals (P_{AC}) and at the DC terminals (P_{DC}) of the converter. These points are shown in Fig. 8. Also, in Fig. 9, adjusted power P_{adj} is shown for the classical AEMs. This is the DC side power compensated for spurious losses:

$$P_{adj}(t) = P_{DC}(t) - \sum_{m,\,n} \Delta P^{m,\,n}(t) \tag{54}$$

where $m = A, B, C$ denotes phases and $n = up, low$ denotes upper and lower arms.

With DEM and AEMs, the difference between P_{PCC} and

P_{AC} is 3 MW, which corresponds to transformer losses (0.3% of the nominal power). However, visible difference exists between P_{DC} values. With the DEM, converter losses amount to approximately 6 MW (difference between P_{AC} and P_{DC}), which corresponds to 0.6% in (53). With the AEMs, the losses are considerably smaller. However, adjusted power P_{adj} is at the same level as P_{DC} of the DEM, which confirms that spurious losses are the source of the mismatch between P_{DC}.

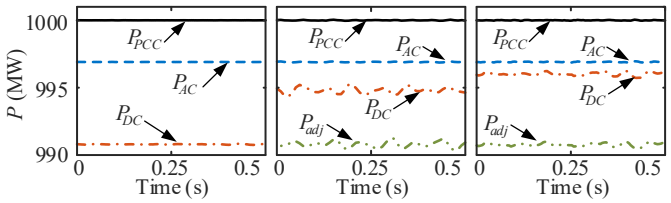

Fig. 9. Transmitted active powers at different points (see Fig. 8).

B. Validation of Analytical Expression of Losses

To validate the analytical expression of spurious power losses, the HVDC link is subjected to nominal power transfer. The waveforms of ΔP in the upper arm of phase A at MMC1 are shown in Fig. 10. Here ΔP_{meas} is the measured value from the simulation and corresponds to (10), ΔP_{calc} is the calculated value and corresponds to (28) for classical AEM 1, and to (34) for classical AEM 2. Instantaneous semiconductor conduction power losses P_{COND} (9) are also shown in Fig. 10 to demonstrate how spurious losses compare to the modeled conduction losses.

Measured and calculated spurious losses match each other well and their values are considerably higher than P_{COND}.

Table II shows the amplitudes of ΔP harmonics calculated using (25)–(27) and (29)–(33) for different power angles φ_{ref} at PCC1 (see Fig. 8). Analytical calculations match simulation results, which validates the analytical expressions.

Same operating conditions are used to demonstrate linear dependency of spurious losses on Δt, Fig. 11. Measured values (markers) match analytical predictions (lines): for classical AEM 1, (27) is considered; and (33) is for classical AEM 2.

Considering results shown in Table II, Fig. 9 to Fig. 11, it is clear that with both classical AEMs the effects of spurious losses are significant and must be removed.

TABLE II
SPURIOUS LOSSES WITH CLASSICAL AEMS (MW)

Operation mode	Measures			Calculations		
	ΔP_0	$\lvert\Delta P_1\rvert$	$\lvert\Delta P_2\rvert$	ΔP_0	$\lvert\Delta P_1\rvert$	$\lvert\Delta P_2\rvert$
Classical AEM 1						
φ_{ref} = +30°	0.56	1.50	2.36	0.54	1.50	2.31
φ_{ref} = 0°	-0.67	2.15	2.70	-0.69	2.15	2.69
φ_{ref} = -30°	-1.91	2.18	2.94	-1.93	2.18	2.96
Classical AEM 2						
φ_{ref} = +30°	0.30	6.81	2.38	0.28	6.89	2.31
φ_{ref} = 0°	-0.87	6.58	2.61	-0.90	6.49	2.69
φ_{ref} = -30°	-2.15	6.38	2.79	-2.17	6.21	2.96

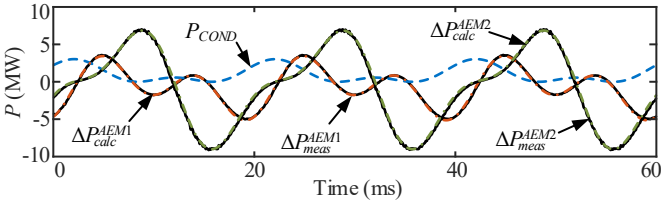

Fig. 10. Power losses in case of nominal power transfer.

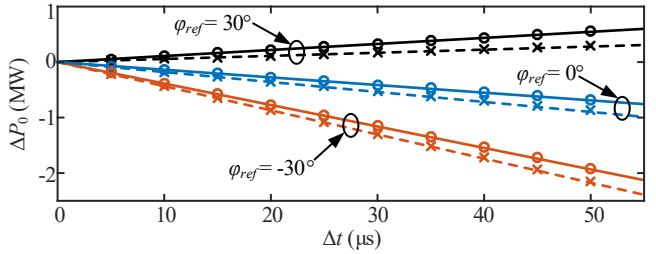

Fig. 11. Effect of Δt on ΔP_0 in different operating conditions. Solid lines and circles – classical AEM 1, dashed lines and crosses – classical AEM 2.

C. Steady-State Behavior Validation

To validate steady-state behavior of all proposed solutions and to see their effect on spurious power losses, the HVDC link is subjected to nominal power transfer. Measured spurious power losses in the upper arm of phase A at MMC1 are shown in Fig. 12. In case of time-step reduction, the Δt used for AEM 1 is 1.5 µs, as calculated with (37). For AEM 2, the Δt is taken as 0.5 µs, which is slightly larger than 0.43 µs provided by (38).

With all solutions, spurious losses are lower than normal conduction losses (that can be seen in Fig. 10). However, neither significant time-step reduction nor extrapolation eliminates losses completely. In these cases, the maximum values of losses are in the order of 0.1 MW. Variable resistance AEM provides the most accurate results, the spurious losses are equal to zero. Equivalent voltage source AEM reduces losses below 1 kW, which is negligible.

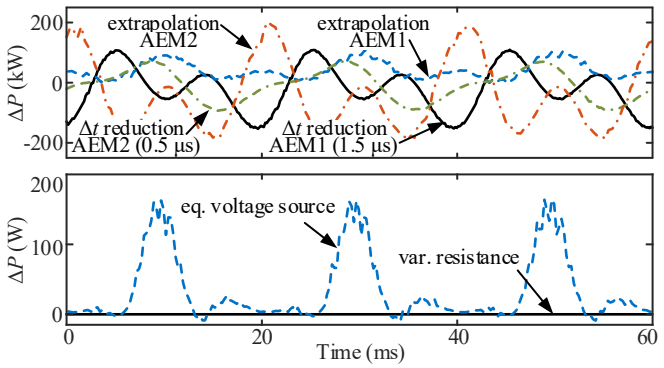

Fig. 12. Spurious power losses with different loss-elimination methods.

D. Transient Behavior Validation

A 200 ms three-phase-to-ground fault at 0.4 s at the PCC1 (see Fig. 8) is used to validate transient behavior of all proposed solutions. Fault resistance is 0.5 Ω. The transient waveforms obtained with DEM are taken as a reference.

Arm voltage of phase-A upper arm of MMC1 is shown in Fig. 13 to Fig. 15: both extrapolation AEMs exhibit high spikes: 25 kV at 0.4387 s (zoom 1) and 180 kV at 0.4526 s

(zoom 2). These moments correspond to sudden changes in reference values in the control system. Another adverse effect of extrapolation AEMs in Fig. 15 is that v_{arm} becomes significantly negative (-18 kV), which is not realistic for MMCs with half-bridge SMs because negative polarization of such SMs would activate antiparallel diodes.

Table III compares the maximal relative deviation of the DC voltage, arm voltage, and capacitor voltage in the upper arm of phase A of MMC 1 during the same simulation with various models. As in [7], relative deviation is computed by dividing the absolute difference between the tested model and the reference by the nominal value of the signal. All models except extrapolation AEMs do not significantly deviate from the reference. Highest deviations are observed in the values of arm voltage. The most accurate match is obtained with time-step reduction because higher-frequency transients can also be represented with such small time-step.

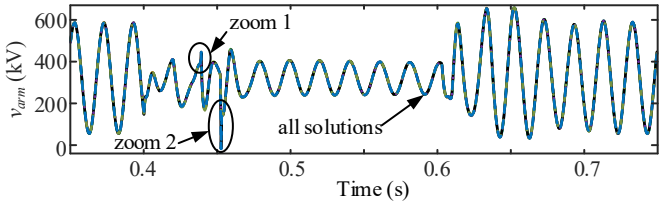

Fig. 13. Arm voltage with different MMC models.

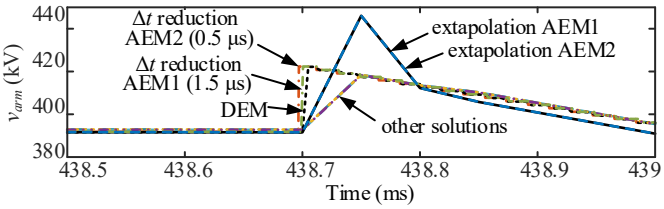

Fig. 14. Arm voltage with different MMC models (zoom 1).

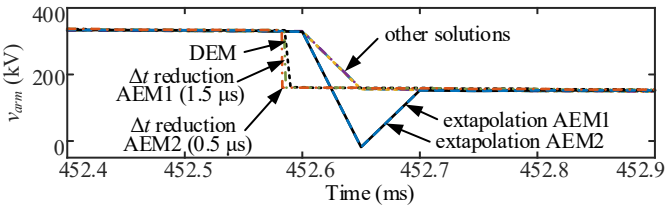

Fig. 15. Arm voltage with different MMC models (zoom 2).

TABLE III
MAXIMAL RELATIVE ERROR (%)

Model	v_{arm}	v_{Ctot}	V_{DC}
Classical AEM 1	2.43	1.29	0.66
Classical AEM 2	2.43	1.40	0.64
Δt reduction for AEM 1 (1.5 µs)	0.72	0.18	0.19
Δt reduction for AEM 2 (0.5 µs)	0.72	0.18	0.19
Extrapolation AEM 1	27.79	0.51	0.35
Extrapolation AEM 2	27.79	0.51	0.35
Variable resistance AEM	2.42	1.18	0.65
Equivalent voltage source AEM	2.42	1.18	0.62

E. Computing Times

To compare computing times of various models, the HVDC link shown in Fig. 8 is simulated during 1 s in steady-state conditions. Results are shown in Table IV. The reference computing time is taken as the one of the classical model AEM 1. Execution time of the DEM is also shown for comparison.

Both classical AEMs have almost identical computing times. Reducing the time-step considerably slows down the simulation (computing times are comparable to that of DEM). The extrapolation AEMs are only slightly slower (less than 6 % difference compared with the reference) due to the presence of additional control blocks. The variable resistance AEM has longer execution time due to the need to refactor the MNE (30% increase in simulation time). Equivalent voltage source AEM is faster than the variable resistance AEM but still about 10% slower than the reference.

TABLE IV
EXECUTION TIME OF DIFFERENT MODELS

Model	Execution time (s)	Relative execution time (%)
Classical AEM 1 (reference)	2.02	100.0
Classical AEM 2	2.05	101.5
Δt reduction for AEM 1 (1.5 µs)	46.99	2324.3
Δt reduction for AEM 2 (0.5 µs)	140.79	6963.4
Extrapolation AEM 1	2.10	103.9
Extrapolation AEM 2	2.14	105.8
Variable resistance AEM	2.69	132.9
Equivalent voltage source AEM	2.28	112.8
DEM (5 µs)	63.75	3152.9

VI. CONCLUSION

This article demonstrates that spurious power loss or generation can occur when using the arm equivalent model of MMC implemented in an EMT-type simulation software. Such power losses are caused by the delay between the solutions of power network and control system equations used in the AEM implementation. Depending on the simulation conditions, spurious losses can represent a significant part of or even exceed total station losses, thus deteriorating the accuracy of simulations.

Several solutions are considered in this paper to remove or reduce the effects of such losses: reducing the time-step, extrapolating arm voltage references, including a variable resistance into the nodal matrix and replacing the variable resistance with an equivalent voltage source. The performances of all proposed solutions are compared on a point-to-point MMC-HVDC link benchmark.

Based on the performances of studied solutions, the variable resistance AEM is recommended for the highest possible accuracy. The equivalent voltage source AEM offers the best compromise between accuracy and computing time.

APPENDIX

A. *Capacitor-Side Power in Classical AEM 2*

From Fig. 3, the following equations can be written:

$$v_{ref}(t) = v_{Ctot}(t)\, s(t) \tag{55}$$

$$i_{Ctot}(t) = i_{arm}(t-\Delta t)\, s(t-\Delta t) \tag{56}$$

Using (55) and (56), capacitor-side power (6) for the classical AEM 2 can be formulated as

$$P_{Ctot\ AEM\ 2}(t)=i_{arm}(t-\Delta t)\,s(t-\Delta t)\frac{v_{ref}(t)}{s(t)} \tag{57}$$

Using (11), (57) is rewritten as

$$P_{Ctot\ AEM\ 2}(t)=i_{arm}(t-\Delta t)\,v_{arm}(t+\Delta t)\frac{s(t-\Delta t)}{s(t)} \tag{58}$$

So, (17) is obtained.

B. *Spurious Losses in the Classical AEM 2*

With small time-steps, exact values of all signals in (58) can be replaced by first-order Taylor series elements at a time-point t:

$$i_{arm}(t-\Delta t)\approx i_{arm}(t)-\Delta t\frac{d}{dt}i_{arm}(t) \tag{59}$$

$$v_{arm}(t+\Delta t)\approx v_{arm}(t)+\Delta t\frac{d}{dt}v_{arm}(t) \tag{60}$$

$$\frac{s(t-\Delta t)}{s(t)}\approx 1-\frac{\Delta t}{s(t)}\frac{d}{dt}s(t) \tag{61}$$

If Π_1 is defined as a product of right-hand sides of (59) and (60), $P_{Ctot\ AEM\ 2}$ can be rewritten:

$$\begin{aligned}\Pi_1(t)=\Delta t\Big[&i_{arm}(t)\frac{d}{dt}v_{arm}(t)-v_{arm}(t)\frac{d}{dt}i_{arm}(t)\Big]\\&+i_{arm}(t)\,v_{arm}(t)-\Delta t^2\frac{d}{dt}i_{arm}(t)\frac{d}{dt}v_{arm}(t)\end{aligned} \tag{62}$$

$$P_{Ctot\ AEM\ 2}(t)\approx\Pi_1(t)\left[1-\frac{\Delta t}{s(t)}\frac{d}{dt}s(t)\right] \tag{63}$$

Neglecting the summands that include multiplication by Δt^2 or Δt^3 in (63) since Δt is considered small:

$$\begin{aligned}P_{Ctot\ AEM\ 2}(t)\approx\ &i_{arm}(t)\,v_{arm}(t)-\Delta t\,v_{arm}(t)\frac{d}{dt}i_{arm}(t)\\&+\Delta t\,i_{arm}(t)\left[\frac{d}{dt}v_{arm}(t)-\frac{v_{arm}(t)}{s(t)}\frac{d}{dt}s(t)\right]\end{aligned} \tag{64}$$

Introducing (64) and (5) to (10):

$$\begin{aligned}P_{AEM\ 2}(t)-P_{Ctot\ AEM\ 2}(t)=&\Delta t\,v_{arm}(t)\frac{d}{dt}i_{arm}(t)\\&-\Delta t\,i_{arm}(t)\left[\frac{d}{dt}v_{arm}(t)-\frac{v_{arm}(t)}{s(t)}\frac{d}{dt}s(t)\right]\end{aligned} \tag{65}$$

This difference constitutes spurious power losses and can be separated into two terms:

$$\Delta P_{AEM\ 2}(t)=\Delta t\,v_{arm}(t)\frac{d}{dt}i_{arm}(t) \tag{66}$$

and

$$\delta P_{AEM\ 2}(t)=-\Delta t\,i_{arm}(t)\left[\frac{d}{dt}v_{arm}(t)-\frac{v_{arm}(t)}{s(t)}\frac{d}{dt}s(t)\right] \tag{67}$$

It is clear that (66) is the same as (18). To obtain (19), it can first be assumed that $s(t)=v_{arm}(t)/v_{Ctot}(t)$ to simplify further analysis. Therefore, (67) is rewritten as

$$\begin{aligned}\delta P_{AEM\ 2}(t)=&\Delta t\,i_{arm}(t)\,v_{Ctot}(t)\frac{d}{dt}\left[\frac{v_{arm}(t)}{v_{Ctot}(t)}\right]\\&-\Delta t\,i_{arm}(t)\frac{d}{dt}v_{arm}(t)\end{aligned} \tag{68}$$

Using the quotient derivative rule and algebraical manipulations, (69) can be obtained

$$\delta P_{AEM\ 2}(t)=-\Delta t\,i_{arm}(t)\frac{v_{arm}(t)}{v_{Ctot}(t)}\frac{d}{dt}v_{Ctot}(t) \tag{69}$$

This is further simplified by approximating $v_{Ctot}(t)\approx V_{DC}$ in the denominator to

$$\delta P_{AEM\ 2}(t)\approx-\Delta t\,i_{arm}(t)\frac{v_{arm}(t)}{V_{DC}}\frac{d}{dt}v_{Ctot}(t) \tag{70}$$

which is identical to (19).

REFERENCES

[1] S. Allebrod, R. Hamerski, and R. Marquardt, "New transformerless, scalable modular multilevel converters for HVDC-transmission," *PESC Record - IEEE Annual Power Electronics Specialists Conference*, Rhodes, Greece2008, pp. 174-179.

[2] K. Jacobs, H. Saad, and S. Dennetiere, "Modelling of semiconductor losses of the Modular Multilevel Converter in EMTP," *2016 IEEE 17th Workshop on Control and Modeling for Power Electronics (COMPEL)*2016, pp. 1-8.

[3] A. Lesnicar and R. Marquardt, "An innovative modular multilevel converter topology suitable for a wide power range," *2003 IEEE Bologna PowerTech - Conference Proceedings*, Bologna, Italy2003, pp. 272-277.

[4] H. Saad, S. Dennetiere, J. Mahseredjian, P. Delarue, X. Guillaud, J. Peralta, and S. Nguefeu, "Modular Multilevel Converter Models for Electromagnetic Transients," *IEEE Trans. on Power Delivery,* vol. 29, pp. 1481-1489, June 2014.

[5] J. Peralta, H. Saad, S. Dennetiere, J. Mahseredjian, and S. Nguefeu, "Detailed and Averaged Models for a 401-Level MMC-HVDC System," *IEEE Trans. on Power Delivery,* vol. 27, pp. 1501-1508, July 2012.

[6] H. Saad, J. Peralta, S. Dennetiere, J. Mahseredjian, J. Jatskevich, J. A. Martinez, A. Davoudi, M. Saeedifard, V. Sood, X. Wang, J. Cano, and A. Mehrizi-Sani, "Dynamic Averaged and Simplified Models for MMC-Based HVDC Transmission Systems," *IEEE Trans. on Power Delivery,* vol. 28, pp. 1723-1730, July 2013.

[7] N. Ahmed, L. Angquist, S. Norrga, A. Antonopoulos, L. Harnefors, and H.-P. Nee, "A Computationally Efficient Continuous Model for the Modular Multilevel Converter," *IEEE Journal of Emerging and Selected Topics in Power Electronics,* vol. 2, pp. 1139-1148, Dec. 2014.

[8] S. Wenig, F. Rojas, K. Schönleber, M. Suriyah, and T. Leibfried, "Simulation framework for DC grid control and ACDC interaction studies based on modular multilevel converters," *IEEE Transactions on Power Delivery,* vol. 31, pp. 780-788, 2016.

[9] J. Xu, A. M. Gole, and C. Zhao, "The use of averaged-value model of modular multilevel converter in DC grid," *IEEE Transactions on Power Delivery,* vol. 30, pp. 519-528, 2015.

[10] H. Saad, K. Jacobs, W. Lin, and D. Jovcic, "Modelling of MMC including half-bridge and Full-bridge submodules for EMT study," *19th Power Systems Computation Conference, PSCC 2016*, Genova, Italy, June 2016, pp. 1-7.

[11] N. Ahmed, L. Ängquist, S. Norrga, H.-P. Nee, and 1, "Validation of the continuous model of the modular multilevel converter with blocking/deblocking capability," *10th IET International Conference on AC and DC Power Transmission (ACDC 2012)*, Birmingham, UK, Dec. 2012, pp. 1-6.

[12] A. Beddard, C. Sheridan, M. Barnes, and T. Green, "Improved accuracy average value models of modular multilevel converters," *IEEE Transactions on Power Delivery,* vol. 31, pp. 2260-2269, 2016.
[13] IEC International Standard, "Power losses in voltage sourced converter (VSC) valves for high-voltage direct current (HVDC) systems – Part 2: Modular multilevel converters",115 p., 2014
[14] S. Norrga, L. Angquist, K. Ilves, L. Harnefors, and H. P. Nee, "Decoupled steady-state model of the modular multilevel converter with half-bridge cells," *6th IET International Conference on Power Electronics, Machines and Drives*, Stevenage, UK, Mar. 2012, pp. 1-6.
[15] J. Beerten, O. Gomis-Bellmunt, X. Guillaud, J. Rimez, A. van der Meer, and D. Van Hertem, "Modeling and control of HVDC grids: A key challenge for the future power system," *Power Systems Computation Conference (PSCC)*, June 2014, pp. 1-21.
[16] A. Stepanov, H. Saad, J. Mahseredjian, and A. Wataré, "Overview of Generic HVDC-MMC Control under Unbalanced Grid Conditions," *International Power Systems Transients Conference (IPST 2017)*, Seoul, South Korea, June 2017, pp. 1-6.
[17] A. Stepanov, H. Saad, U. Karaagac, and J. Mahseredjian, "Initialization of Modular Multilevel Converter Models for the Simulation of Electromagnetic Transients," *IEEE Transactions on Power Delivery,* 2018.
[18] J. Mahseredjian, S. Dennetière, L. Dubé, B. Khodabakhchian, and L. Gérin-Lajoie, "On a new approach for the simulation of transients in power systems," *Electric Power Systems Research,* vol. 77, pp. 1514-1520, Sep. 2007.
[19] P. S. Jones and C. C. Davidson, "Calculation of power losses for MMC-based VSC HVDC stations," *15th European Power Electronics and Applications Conference (EPE)*, Sep. 2013, pp. 1-10.
[20] P. Kundur, *Power System Stability and Control*: McGraw Hill, 1994.
[21] CIGRE Working Group B4.57, "Guide for the Development of Models for HVDC Converters in a HVDC Grid",221 p., 2014